



Orientation Relationships in FeMnNiAl Governed by Martensitic Substructure

Ahmed Sameer Khan Mohammed¹ · R. Sidharth¹ · Wael Abuzaid² · Hiroshi Akamine³ · Minoru Nishida³ · Huseyin Sehitoglu¹

Received: 7 March 2023 / Revised: 28 June 2023 / Accepted: 1 August 2023 / Published online: 24 August 2023
© ASM International 2023

Abstract This study establishes the Orientation Relationship (OR) between the austenitic and martensitic phases of the new Shape Memory Alloy (SMA) FeMnNiAl from both experiments and analytical modeling. Through Transmission Electron Microscopy (TEM) and Electron Back-Scatter Diffraction, three distinct ORs, namely the Nishiyama-Wassermann (N-W), Pitsch, and Kurdjumov–Sachs (K-S) ORs are established. The observations of non-unique ORs are explained using the energy-minimization theory of martensite revealing dependence of OR on the internal morphology of the martensitic phase, whether twinned or stacking-faulted. It is shown that the twin-variants of an internally twinned martensitic structure individually explain the Pitsch and K-S ORs. The N-W OR was observed in a stacking-faulted substructure of martensite. Through a novel extension to the energy-minimization theory for stacking-faulted substructures, the N-W OR is explained. Thus, the current

study challenges the notion of OR as a material-characteristic and reveals a dependence of the OR on the internal substructure of the martensitic phase in SMAs, further establishing the OR for the new SMA FeMnNiAl.

Keywords Orientation relationship · Shape Memory Alloy · Twinning · Stacking fault

Introduction

Materials of today exhibit microstructures that most often feature multiple phases, with these phases exercising strong influence on the materials' properties. For instance, precipitate-phases in structural alloys elevate the mechanical strength [1–4], second-phase fiber/particle-reinforcements within a binding matrix-phase dictate the stiffness of composite materials [5–7], and stimuli-induced nucleation of a product-phase within a primary parent-phase can attribute high-deformability in several functional materials [8–11]. This study focuses on a class of functional materials known as Shape Memory Alloys (SMA) where a mechanically induced phase-transformation from a parent Austenitic (A) phase to a product Martensitic (M) phase attributes functional characteristics relevant in several applications spanning biomedical, automotive, and aerospace domains [12–14]. Specifically, this study uses experiments and theory to expound the relative Orientation Relationship (OR) between the lattices of the A and M phases in SMAs.

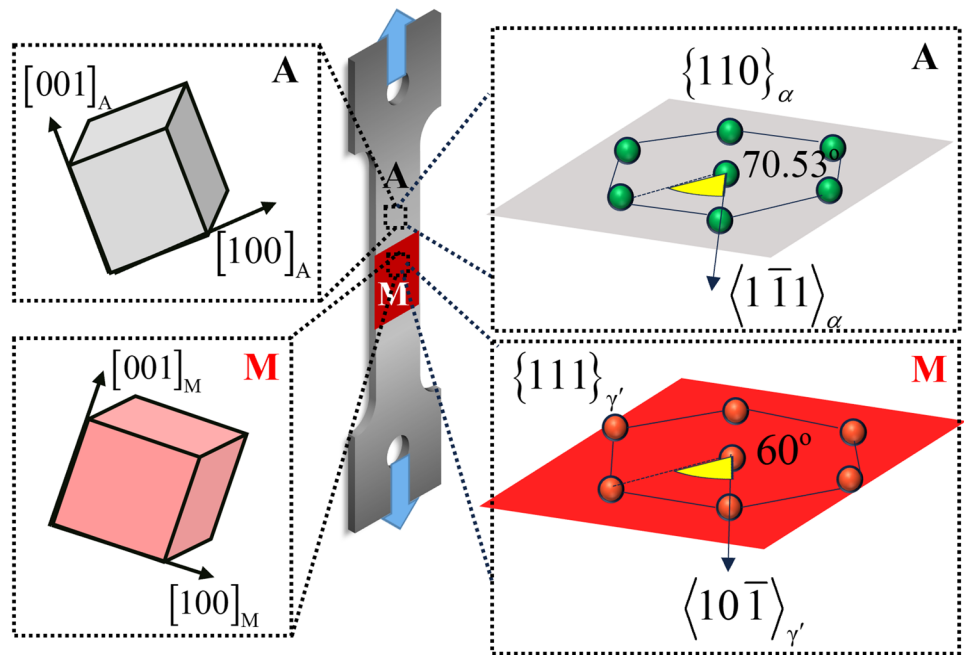
This Orientation Relationship (OR) between the A and M phases are generally described by two parallelism conditions: (i) the first parallelism is between two crystallographic planes, one in the A-lattice $(hkl)_A$ and another in the M-lattice $(h'k'l')_M$, (ii) the second parallelism is between two crystallographic directions, one in

This article is an invited submission to *Shape Memory and Superelasticity* selected from presentations at the 12th European Symposium on Martensitic Transformations (ESOMAT 2022) held September 5–9, 2022 at Hacettepe University, Beytepe Campus, Ankara, Turkey, and has been expanded from the original presentation. The issue was organized by Prof. Dr. Benat Koçkar, Hacettepe University.

✉ Ahmed Sameer Khan Mohammed
am14@illinois.edu

- ¹ Department of Mechanical Science and Engineering, University of Illinois at Urbana-Champaign, 1206 W Green St, Urbana, IL 61801, USA
- ² Department of Mechanical Engineering, American University of Sharjah, PO Box 26666, Sharjah, United Arab Emirates
- ³ Department of Advanced Materials Science and Engineering, Faculty of Engineering Sciences, Kyushu University, Kasuga, Fukuoka 816-8580, Japan

Fig. 1 Superelastic phase-transformation behavior of parent Austenite (A) to Martensite (M) schematically represented within a dog-bone specimen; the focus of the study is on the lattice-orientation relationship between the two crystal structures, generally established as a parallelism between a crystallographic direction and a crystallographic plane; for the case of Body-Centered-Cubic (BCC α) austenite and Face-Centered-Cubic (FCC γ') martensite, the directions and planes are illustrated



the A-lattice $[uvw]_A$ and another in the M-lattice $[u'v'w']_M$ (refer Fig. 1). Such ORs have long been established experimentally for several SMAs [15–22] and are often tacitly attributed to be a property of the material. The OR can equivalently be stated as an invariance of the two elements in the parent phase involved in the parallelism condition—a crystallographic plane $(hkl)_A$ and a crystallographic direction $[uvw]_A$ —during the transformation. Therefore, the OR can be specified by the invariant plane $(hkl)_A$ and direction $[uvw]_A$ in the parent phase, or more generally by the families $\{hkl\}_A$ and $\langle uvw \rangle_A$.

Understanding the OR in SMAs is particularly critical to address the challenge of fatigue in this material class. Fatigue in SMAs occurs by a mechanism of transformation-induced slip where slip-dislocations are emitted in the A phase from the A-M transformation front. And it is well-established that the activated slip-system in the A phase exhibits a close agreement with internal interfaces within the M phase [23–28]. Thus, to predict the propensity for slip-emission and consequently of fatigue, it is necessary to address the relative orientation of the slip-planes in the A-phase in relation to the internal interfaces of the M-phase. Although ORs for multiple SMAs have been proposed and well-characterized experimentally, there are few knowledge-gaps that remain in these relationships, listed as follows:

- Relation of OR to internal morphology of the M-phase: The ORs are generally specified for the SMA system in a manner that is independent from the internal structure

of the martensite, whether twinned or stacking faulted. Particularly if the M-phase is internally twinned, it is important to know how the OR connects with the orientation of each of the twin variants.

- Lattice-correspondence and OR: In converting the A-crystal structure to the M-crystal structure, there are known lattice-correspondences that are proposed. These correspondences describe which crystallographic vector-basis of the parent transforms into the unit cell crystallographic basis of the martensite. It is unclear how the lattice-correspondences are linked to the OR. If the lattice-correspondence describes a relationship between crystallographic directions in the A-phase and M-phase (as described previously), it is necessary to understand how it differs from the observed OR.
- Exactness of the OR: It is important to know if the parallelism conditions used to define the OR are exact in nature or if there is a tolerance of a few degrees in them. The existence of such tolerance and their magnitude is essential to understand the gradient of crystal structures at the transformation front.

This study focuses on addressing all aforementioned issues. The framework is developed from the energy-minimization theory of martensite, typically used to predict the crystallography of habit planes. The study target is chosen from the new FeMnNiAl SMA system, specifically the alloy with composition $\text{Fe}_{43.5}\text{Mn}_{34}\text{Al}_{15}\text{Ni}_{7.5}$. This SMA alloy has been of recent interest in the field as a promising inexpensive alternative to NiTi, offering a temperature-invariant transformation stress and large transformation strains exceeding

10% [29–32]. This system has thus far been reported to exhibit the Pitsch OR [33–35] and this study investigates the OR further. Furthermore, there is the added advantage of working with cubic crystal structures in the A and M phases. With a cubic structure, the reciprocal space lattice is in perfect alignment with the real-space lattice. This affords the convenience of discussing alignment of crystallographic planes and directions in an interchangeable manner. In other words, the parallelism of two crystallographic planes $(hkl)_A$ and $(mnp)_M$ is exactly equivalent to stating parallelism of the normal crystallographic directions $[hkl]_A$ and $[mnp]_M$. In FeMnNiAl, the austenitic phase is Body-Centered-Cubic and the martensitic phase is Face-Centered-Cubic. These structures provide an ideal starting case to examine the OR between the A and M phases. The layout of the paper is as follows. Sect. “Methodology and Results” develops the methodology and presents the experimental/model results, Sect. “Discussion” discusses the implications and Sect. “Conclusions” presents the conclusions.

Methodology and Results

This section begins with the experimental observations of ORs between the BCC (α) austenite (lattice constant $a_A = 2.903 \text{ \AA}$) and FCC (γ') martensite (lattice constant $a_M = 3.672 \text{ \AA}$) in $\text{Fe}_{43.5}\text{Mn}_{34}\text{Al}_{15}\text{Ni}_{7.5}$ (the experimentally measured lattice constants are reported in ref [30]). Results from Selected Area Electron Diffraction (SAED) obtained from Transmission Electron Microscopy (TEM) and from Electron Backscatter Diffraction (EBSD) are presented. Then the predictive framework for the OR is elaborated starting from the lattice correspondence between the phases. The energy minimization theory of martensite is outlined and applied to the problem. The resulting ORs from the theory are compared with the experimentally observed ORs.

Experimental Observations

Compression-tested samples of FeMnNiAl were used to characterize the OR. These samples exhibited stress-induced transformation at room-temperature. TEM samples were milled out of transformed region using Focused Ion Beam (FIB) milling and thinned to electron-transparency. The results of the TEM imaging and SAED are presented in Fig. 2. The martensite is observed to form in a diamond-shaped self-accommodation morphology as shown in Fig. 2a consistent with prior reports in this system [35]. The diamond-morphology consists of 4 distinct Habit-Plane Variants (HPVs) with four planar transformation fronts. These variants form together and alongside to

comprise the diamond-shape. Other independent HPVs forming parallel to the sides of the diamond-martensite are also observed. SAED patterns are collected from multiple regions as indicated in figures (b-e). When the austenite crystal structure is aligned to the $[110]_\alpha$ zone axis (Fig. 2b), the martensite crystal structure is also on an aligned zone-axis of $[211]_{\gamma'}$. This yields the SAED pattern shown in Fig. 2d. There is also the diffraction signature from fine B2 precipitates in the matrix, shown in Fig. 2b. By placing the SAED aperture on a region that includes both A and M phases, the combined diffraction patterns from both phases are obtained and used to infer the OR. It is found that the planes $(\bar{1}11)_{\gamma'} \parallel (\bar{1}10)_\alpha$ are nearly parallel as their diffraction spots are at close proximity to each other. And, as noted before, the crystallographic zone-axes $[211]_{\gamma'} \parallel [110]_\alpha$ are aligned. Therefore for this OR, we have $(hkl)_A = (\bar{1}10)_\alpha$ and $[uvw]_A = [110]_\alpha$. More generally, the OR is expressed based on the family of corresponding planes and directions i.e., $\{hkl\}_A = \{\bar{1}10\}_\alpha$ and $\langle uvw \rangle_A = \langle 110 \rangle_\alpha$. This OR is known as the Nishiyama-Wassermann OR [36].

The ORs were further examined using EBSD. Figure 3 presents an EBSD map on the surface of a deformed FeMnNiAl sample. The EBSD scan provides the Euler-angles at each spatial location as indicated—a triad $(\varphi_{1A}, \Phi_A, \varphi_{2A})$ for austenite and $(\varphi_{1M}, \Phi_M, \varphi_{2M})$ for martensite, with respect to a common global frame of reference $x_1 - y_1 - z_1$. These measured Euler angles are used to determine the OR between the phases. The orientation of each phase is given by the rotation matrices Q_A, Q_M , respectively, the columns of which represent the coordinates of the crystallographic vectors of each respective phase in the global frame. The Euler angles are obtained in the extrinsic “zxz” convention and the respective rotation matrices for both phases are given by:

$$Q_{A,M} = \begin{pmatrix} \cos\varphi_{1A,M} & \sin\varphi_{1A,M} & 0 \\ -\sin\varphi_{1A,M} & \cos\varphi_{1A,M} & 0 \\ 0 & 0 & 1 \end{pmatrix} \begin{pmatrix} 1 & 0 & 0 \\ 0 & \cos\Phi_{A,M} & \sin\Phi_{A,M} \\ 0 & -\sin\Phi_{A,M} & \cos\Phi_{A,M} \end{pmatrix} \begin{pmatrix} \cos\varphi_{2A,M} & \sin\varphi_{2A,M} & 0 \\ -\sin\varphi_{2A,M} & \cos\varphi_{2A,M} & 0 \\ 0 & 0 & 1 \end{pmatrix} \tag{1}$$

The OR is visualized in a stereographic projection as illustrated in Fig. 4. All unit crystallographic directions are projected onto a selected crystallographic plane ($(0\bar{1}1)$ in the case shown in Fig. 4a) and visualized as a 2D plot of points (Fig. 4b). The closest points from the A phase and M phase correspond to the most closely aligned/parallel directions between the phases and are used to determine the OR. The crystallographic orientation of the FCC (M)

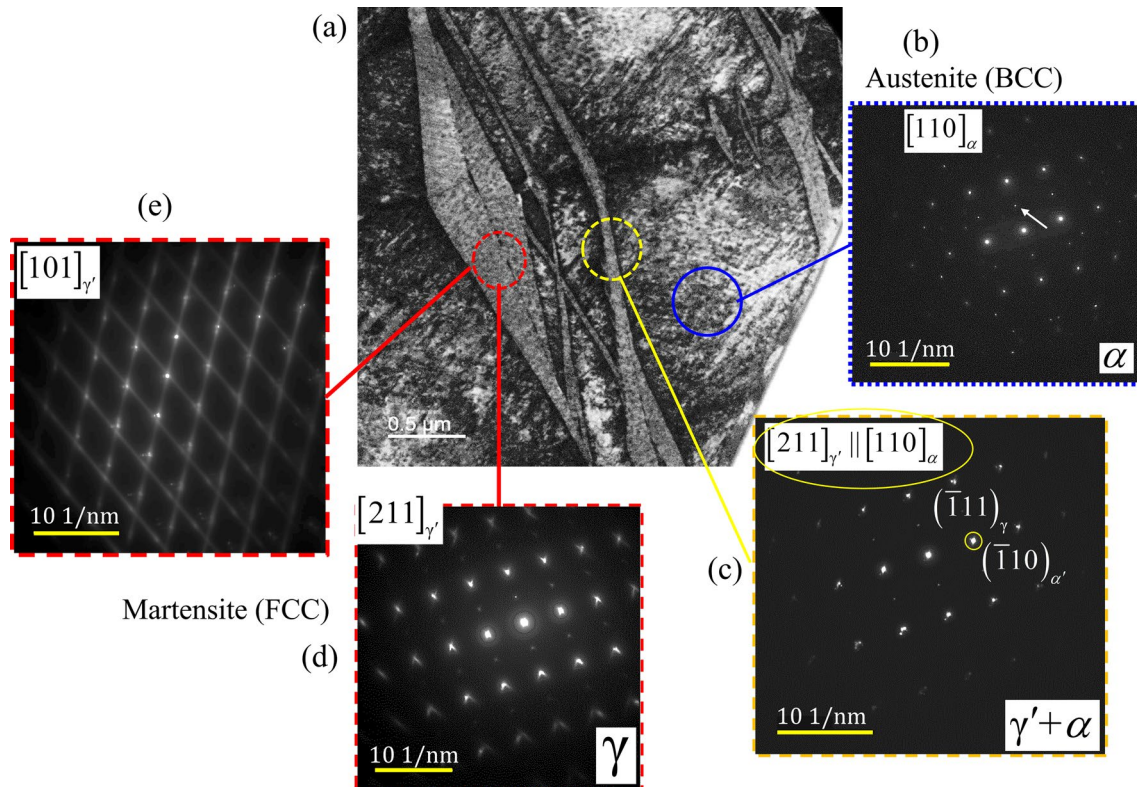


Fig. 2 TEM observation of orientation-relationship between austenite (BCC α) and martensite (FCC γ') in FeMnNiAl: **a** Bright-field TEM image showing the transformed martensite, forming in a “diamond-shape” self-accommodating morphology; other parallel bands of transformed martensite can also be seen. **b** Selected-Area Electron Diffraction (SAED) pattern taken from the austenite phase (BCC α) including B2 precipitates, the zone-axis is $[110]_{\alpha}$ and extra spot marked with white single arrow is derived from B2 precipitates. **c** SAED pattern from both the austenite (BCC α) including B2 precipi-

tates and martensite (FCC γ') phases, **d** SAED from the martensite phase (FCC γ'), where the zone-axis is parallel to $[211]_{\gamma'}$; the SAED from (c) consequently illustrates a parallelism between the zone-axes $[211]_{\gamma'} \parallel [110]_{\alpha}$ and the planes $(\bar{1}11)_{\gamma'} \parallel (\bar{1}10)_{\alpha}$ (from near coincidence of the corresponding diffraction spots), confirming the Nishiyama-Wassermann orientation relationship **e** SAED pattern tilted about 35 degrees around from (d), the zone-axis is, showing a “streaking” nature and thus the prevalence of stacking-faults in the underlying martensite

phase is taken as reference, and the BCC (A) orientation is plotted relative to it. A unit vector along the crystallographic direction $C_A = a_A[uvw]_A$ in the austenite phase has the components (x_A, y_A) in the stereographic projection where:

$$\begin{pmatrix} x_A \\ y_A \\ z_A \end{pmatrix} = \frac{1}{\|C_A\|} \begin{pmatrix} 0 & 1/\sqrt{2} & 1/\sqrt{2} \\ -1 & 0 & 0 \\ 0 & -1/\sqrt{2} & 1/\sqrt{2} \end{pmatrix} Q_M^T Q_A \begin{pmatrix} u \\ v \\ w \end{pmatrix} \quad (2)$$

A unit vector along the crystallographic direction $C_M = a_M[rst]_M$ in the martensite phase has the components (x_M, y_M) in the stereographic projection where:

$$\begin{pmatrix} x_M \\ y_M \\ z_M \end{pmatrix} = \frac{1}{\|C_M\|} \begin{pmatrix} 0 & 1/\sqrt{2} & 1/\sqrt{2} \\ -1 & 0 & 0 \\ 0 & -1/\sqrt{2} & 1/\sqrt{2} \end{pmatrix} \begin{pmatrix} r \\ s \\ t \end{pmatrix} \quad (3)$$

Results of the relative orientations from EBSD site-pairs 2 and 3 from Fig. 3 are plotted in Fig. 5a, b, respectively. It is found that the Pitsch OR is followed at site 2 where $\{hkl\}_A = \{112\}_{\alpha}$ and $\langle uvw \rangle_A = \langle 1\bar{1}0 \rangle_{\alpha}$. Whereas at site 3, the Kurdjumov–Sachs OR is followed, where $\{hkl\}_A = \{110\}_{\alpha}$ and $\langle uvw \rangle_A = \langle 1\bar{1}1 \rangle_{\alpha}$ [36]. All three observed ORs are listed in Table 1.

Theoretical Predictions: Twinned Martensite

To predict the OR, the crystallography of the transformed martensite must be predicted in relation to the parent austenitic phase. The Bain lattice-correspondence provides the relation of the martensitic crystal structure with the austenite parent. This correspondence is such that the parent A-phase requires the least stretch, alternatively called the “Bain strain,” to transform to the M-phase crystal structure. For the BCC parent and FCC transformed

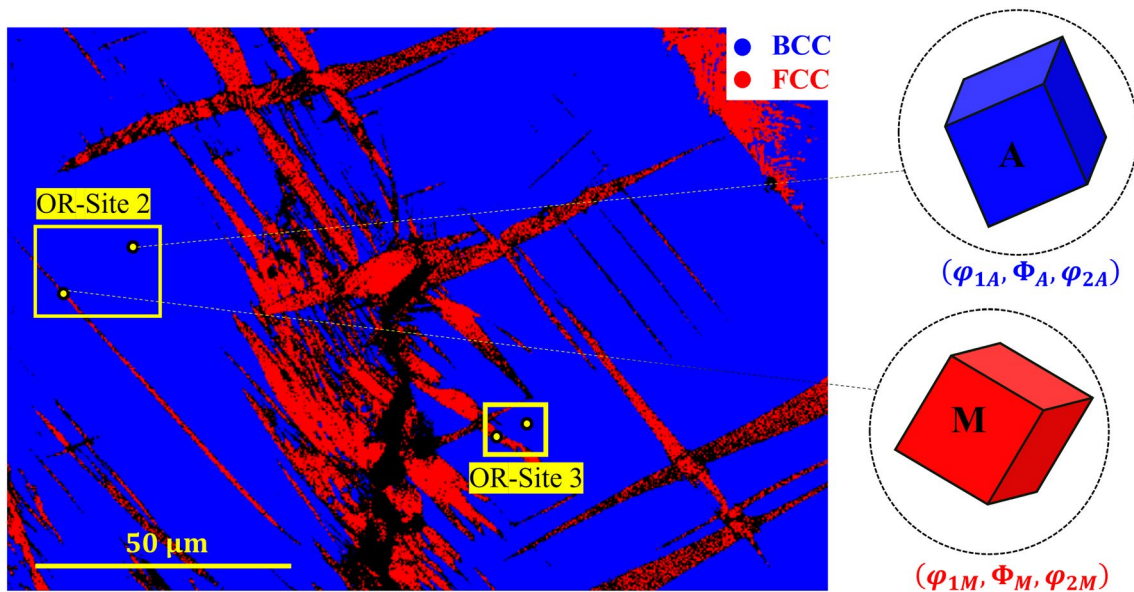


Fig. 3 Electron Back-Scatter Diffraction (EBSD) map of deformed FeMnNiAl sample around a crack; the local Euler-angles $(\varphi_1, \Phi, \varphi_2)$ of the austenite (A, in blue) and martensite (M, in red) lattices are

obtained pairwise sites (sites 2 and sites 3) and mutually compared to deduce the relative orientation relationship

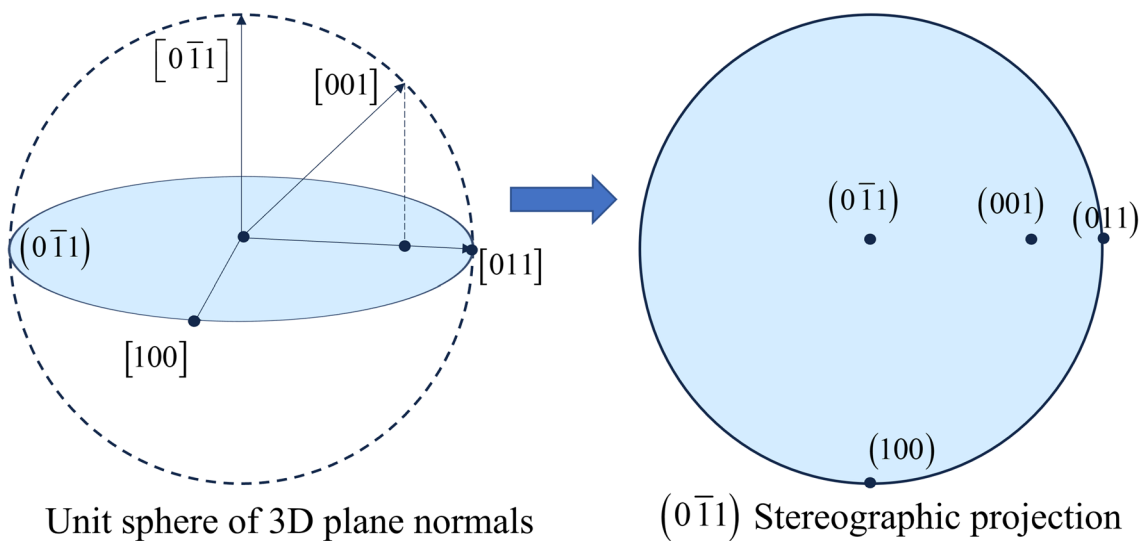


Fig. 4 Concept of a stereographic projection illustrating how the 3-dimensional plane normal are projected to obtain a 2-dimensional visualization; this approach is useful to compare the orientations of austenite and martensite lattices in this study

martensite, the lattice correspondence and required Bain strains are shown in Fig. 6. The lattice correspondences are represented by the equations:

$$\begin{aligned}
 \langle 1\bar{1}0_A \rangle &\leftrightarrow \langle 100_M \rangle \\
 \langle 110_A \rangle &\leftrightarrow \langle 010_M \rangle \\
 \langle 001_A \rangle &\leftrightarrow \langle 001_M \rangle
 \end{aligned}
 \tag{4}$$

Note that although a crystallographic family of directions is used to represent the correspondence in (4), an orthogonal triad must be chosen for the directions in the austenite phase that become the crystallographic basis of the martensite crystal structure. There are 3 such unique correspondences. They are given by the following correspondence matrices Q^{LAT} in Eq. (5) below. The rows of the matrix represent the lattice vectors of the austenite phase that transform to the

Table 1 Observed Orientation Relationships in FeMnNiAl

Label	Invariant plane in austenite (A) $\{hkl\}_A$	Invariant direction in austenite (A) $\langle uvw \rangle_A$	Parallelism condition between phases
Nishiyama-Wassermann	$\{\bar{1}\bar{1}0\}_\alpha$	$\langle 110 \rangle_\alpha$	$\{110\}_\alpha \parallel \{\bar{1}\bar{1}1\}_{\gamma'}$ $\langle 110 \rangle_\alpha \parallel \langle 211 \rangle_{\gamma'}$
Pitsch	$\{112\}_\alpha$	$\langle \bar{1}\bar{1}0 \rangle_\alpha$	$\{112\}_\alpha \parallel \{110\}_{\gamma'}$ $\langle \bar{1}\bar{1}0 \rangle_\alpha \parallel \langle 001 \rangle_{\gamma'}$
Kurdjumov–Sachs	$\{110\}_\alpha$	$\langle \bar{1}\bar{1}1 \rangle_\alpha$	$\{110\}_\alpha \parallel \{111\}_{\gamma'}$ $\langle \bar{1}\bar{1}1 \rangle_\alpha \parallel \langle 10\bar{1} \rangle_{\gamma'}$

crystallographic basis in the martensite phase, $[100]_M - [010]_M - [001]_M$ respectively. For example, in the first correspondence matrix Q_1^{LAT} , the orthogonal triad of lattice vectors $[100]_A - [0\bar{1}\bar{1}]_A - [011]_A$ in the austenite phase transform to the crystallographic basis vectors $[100]_M - [010]_M - [001]_M$ in the martensite phase.

$$Q_1^{LAT} = \begin{pmatrix} 1 & 0 & 0 \\ 0 & 1 & -1 \\ 0 & 1 & 1 \end{pmatrix}; Q_2^{LAT} = \begin{pmatrix} 0 & 1 & 0 \\ -1 & 0 & 1 \\ 1 & 0 & 1 \end{pmatrix}; Q_3^{LAT} = \begin{pmatrix} 0 & 0 & 1 \\ 1 & -1 & 0 \\ 1 & 1 & 0 \end{pmatrix} \tag{5}$$

The corresponding unitary rotation matrices are given by Q^{ROT} as follows:

$$Q_1^{ROT} = \begin{pmatrix} 1 & 0 & 0 \\ 0 & 1/\sqrt{2} & -1/\sqrt{2} \\ 0 & 1/\sqrt{2} & 1/\sqrt{2} \end{pmatrix}; Q_2^{ROT} = \begin{pmatrix} 0 & 1 & 0 \\ -1/\sqrt{2} & 0 & 1/\sqrt{2} \\ 1/\sqrt{2} & 0 & 1/\sqrt{2} \end{pmatrix}; \tag{6}$$

$$Q_3^{ROT} = \begin{pmatrix} 0 & 0 & 1 \\ 1/\sqrt{2} & -1/\sqrt{2} & 0 \\ 1/\sqrt{2} & 1/\sqrt{2} & 0 \end{pmatrix}$$

The corresponding stretch tensors for the above correspondences, expressed in the crystallographic basis of the A phase are given by the equation:

$$U_1 = \begin{pmatrix} \eta_2 & 0 & 0 \\ 0 & \eta_1 & 0 \\ 0 & 0 & \eta_1 \end{pmatrix}; U_2 = \begin{pmatrix} \eta_1 & 0 & 0 \\ 0 & \eta_2 & 0 \\ 0 & 0 & \eta_1 \end{pmatrix}; U_3 = \begin{pmatrix} \eta_1 & 0 & 0 \\ 0 & \eta_1 & 0 \\ 0 & 0 & \eta_2 \end{pmatrix} \tag{7}$$

where $\eta_1 = a_M/(a_A\sqrt{2})$, $\eta_2 = a_M/a_A$.

Given the lattice-correspondences, the energy-minimization theory of martensite can be used to determine the relative orientation between the M and A phases. A brief summary of the theory is provided here and the reader is referred to refs. [37, 38] for further details. Based on the theory, the M-phase forms within the A-phase such that it follows an Invariant Plane Strain (IPS) deformation, so that

the strain-energy is minimized. And to achieve such a deformation, the M-phase is generally internally twinned. In such a case, there are two variants of martensite U_i and U_j with $i \neq j$ that form and the orientation of both variants must be considered individually. The fundamental equations of the theory are as follows:

$$R_{ij}U_j - U_i = \vec{a} \otimes \hat{n} \tag{8}$$

$$R_h[fR_{ij}U_j + (1-f)U_i] = I + \vec{b} \otimes \hat{m} \tag{9}$$

where U_i and U_j are the two variants considered, f is the volume-fraction of U_j , R_h, R_{ij} are rotation tensors, I is the identity tensor, \vec{a} is the twinning shear, \hat{n} is the twinning plane between the variants, \vec{b} is the effective transformation shear of the IPS deformation and \hat{m} is the habit plane of the transformation. Using Eq. (8) in (9) we have the simpler form:

$$R_h[U_i + f(\vec{a} \otimes \hat{n})] = I + \vec{b} \otimes \hat{m} \tag{10}$$

The theory is well-developed to the point that, given a choice of two variants U_i and U_j , every other term in the Eq. (9) can be determined. In other words, all Habit Plane Variants (HPVs) of the transformation can be determined starting from the choice of U_i and U_j . Only those HPVs are considered that yield the twinning normal to be parallel to $\langle 111 \rangle$ in the M phase and the twinning shear direction parallel to the corresponding $\langle 112 \rangle$ twinning direction on the plane. In other words, it must be checked that:

$$\hat{n}_{FCC} = Q_i^{ROT}U_i^{-1}\hat{n} / \|U_i^{-1}\hat{n}\| \in \{111\}$$

$$\vec{a}_{FCC} = Q_i^{ROT}\vec{a} / \|U_i^{-1}\hat{n}\| \in \sqrt{3}/6\{112\} \tag{11}$$

By ensuring \vec{a}_{FCC} satisfies Eq. (11), it is ensured that $\|a_{FCC}\| = 0.707$ which is the twinning shear in FCC. It is found that 24 independent HPV solutions exist, all

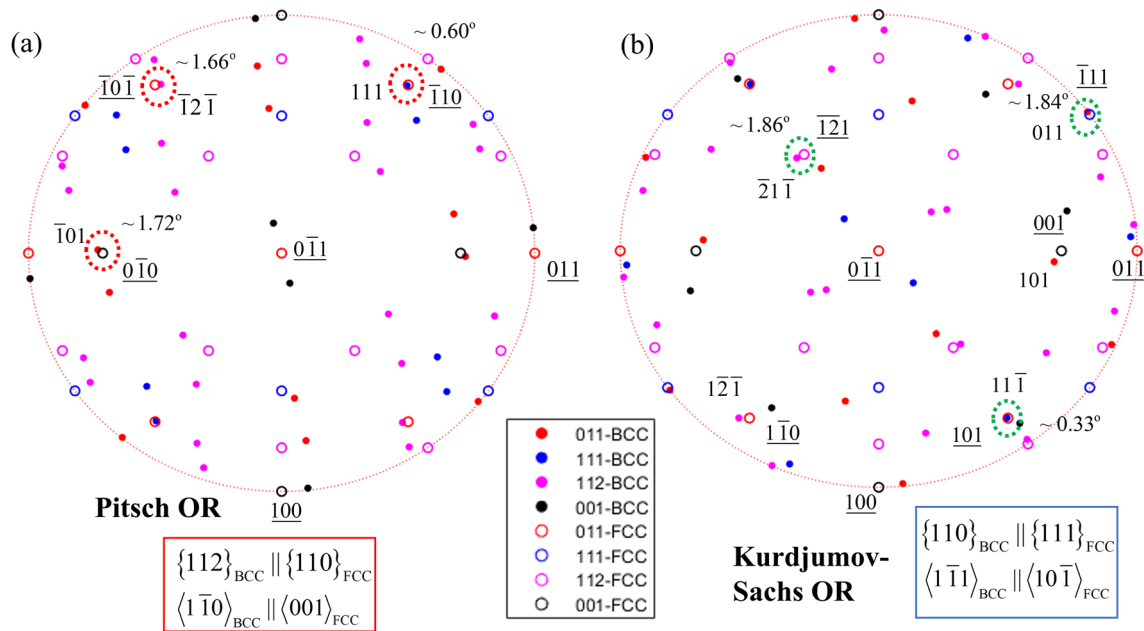


Fig. 5 Overlapped stereographic projection of BCC austenite (filled circles) and FCC martensite (open circles) from EBSD results; **a** the relative orientations obtained from OR Site 2 (refer Fig. 3) are plotted; Based on the nearest coincident directions, the Pitsch OR is

observed **b** the relative orientations obtained from OR Site 3 (refer Fig. 3) are plotted; Based on the nearest coincident directions, the Kurdjumov–Sachs OR is observed

within the family of habit planes $\{0.1678, 0.6455, 0.7451\}$, consistent with prior predictions in ref. [35]. Considering one of the HPV solutions in this family, say with $i = 2$ and $j = 3$, the deformation gradients $F_{M2} = R_h U_2$ and $F_{M3} = R_h R_{ij} U_j$ are calculated. These deformation gradients represent the mapping between the crystal structure of the austenite to form each individual twin variant. To determine which OR is followed by each variant, the condition of invariance is checked for the crystallographic planes and directions corresponding to each OR (listed

in Table 1). For instance, to check if the variant with deformation gradient F_{M2} follows the Pitsch OR, the invariance of a plane normal $\hat{n} \in \{112\}_\alpha$ and unit vector $\hat{v} \in \langle 1\bar{1}0 \rangle_\alpha$ must be checked. The plane normal \hat{n} and the unit vector \hat{v} transform under the deformation gradient as per the following equation:

$$\hat{n}_2 = \frac{F_{M2}^{-T} \hat{n}}{\|F_{M2}^{-T} \hat{n}\|}; \hat{v}_2 = \frac{F_{M2} \hat{v}}{\|F_{M2} \hat{v}\|} \tag{12}$$

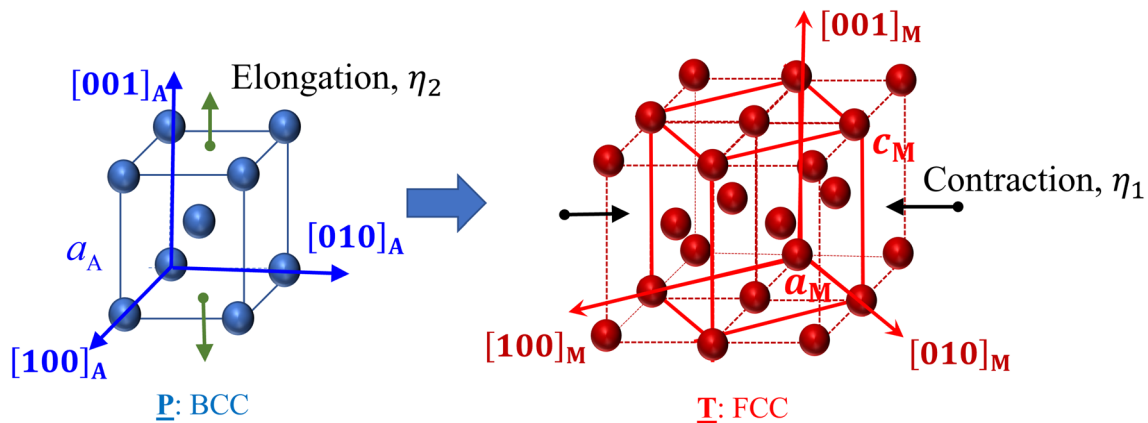


Fig. 6 Bain correspondence and Bain strains η_1, η_2 corresponding to the right stretch-tensor U , required to transform the parent austenitic phase (BCC) to martensite (FCC)

An error-function Δe_{PCH} is computed as follows,

$$\Delta e_{PCH} = \sqrt{(\cos^{-1}|\hat{n}_2 \cdot \hat{n}|)^2 + (\cos^{-1}|\hat{v}_2 \cdot \hat{v}|)^2} \quad (13)$$

Similar error-functions are computed to check for the Kurdjumov–Sachs OR, Δe_{KS} , and Nishiyama-Wassermann OR, Δe_{NW} , by selecting the respective plane \hat{n} and direction \hat{v} accordingly from Table 1. The least magnitude of the error within the set $\{\Delta e_{PCH}, \Delta e_{NW}, \Delta e_{KS}\}$ decides the OR. It is found that in all the HPV solutions of internally twinned martensites, one of the twin variants follows the Pitsch OR, while the other follows the Kurdjumov–Sachs OR. These predictions explain the ORs observed from EBSD in Fig. 5. To further confirm the OR, the stereographic projection of both the BCC and FCC phases are plotted. An example of a HPV solution with variants ($i = 2, j = 3$) is used to illustrate the model predicted results. The variant U_2 , with the deformation gradient F_{M2} follows the Pitsch OR, while variant U_3 with the deformation gradient F_{M3} follows the Kurdjumov–Sachs OR.

The stereographic projections are plotted with reference to the parent BCC phase, and a $(001)_\alpha$ projection is chosen. In this standard projection, the unit directions in the BCC crystal structure can be plotted trivially. For the FCC crystal structure, a unit vector along the crystallographic direction $C_M = a_M[uvw]_M$ within variant U_2 has the components (x_M, y_M) in the stereographic projection given by:

$$\vec{v}_S = a_A F_{M2} (Q_2^{LAT})^T \begin{pmatrix} u \\ v \\ w \end{pmatrix} \quad (14)$$

$$\begin{pmatrix} x_M \\ y_M \\ z_M \end{pmatrix} = \vec{v}_S / \|\vec{v}_S\| \quad (15)$$

The stereographic projections for the variants U_2 and U_3 for the twinned martensite HPV are plotted in Figs. 7 and 8, respectively, illustrating the Pitsch OR and Kurdjumov–Sachs OR.

Theoretical Predictions: Stacking-Faulted Martensite

In addition to twinning, formation of stacking-faults is an alternative Lattice-Invariant-Deformation (LID) mode for the transformation. And given the observations of stacking faults from the SAED results in Fig. 2e, a predictive model for the OR of such a morphology is developed. A novel theory is proposed for the case of stacking-faulted martensite, proposed for the first time to the best of the authors’ knowledge. Consider the martensite forming as a single variant U_i with periodically spaced stacking-faults on planes \hat{n} and direction of faulting is parallel to the Shockley-partial Burgers vector on the plane \vec{a} . Let the faults be periodically spaced by magnitude d . The stacking-faulted martensite is represented schematically in Fig. 9a. Then, for the martensite to follow an IPS deformation, the following condition must be satisfied:

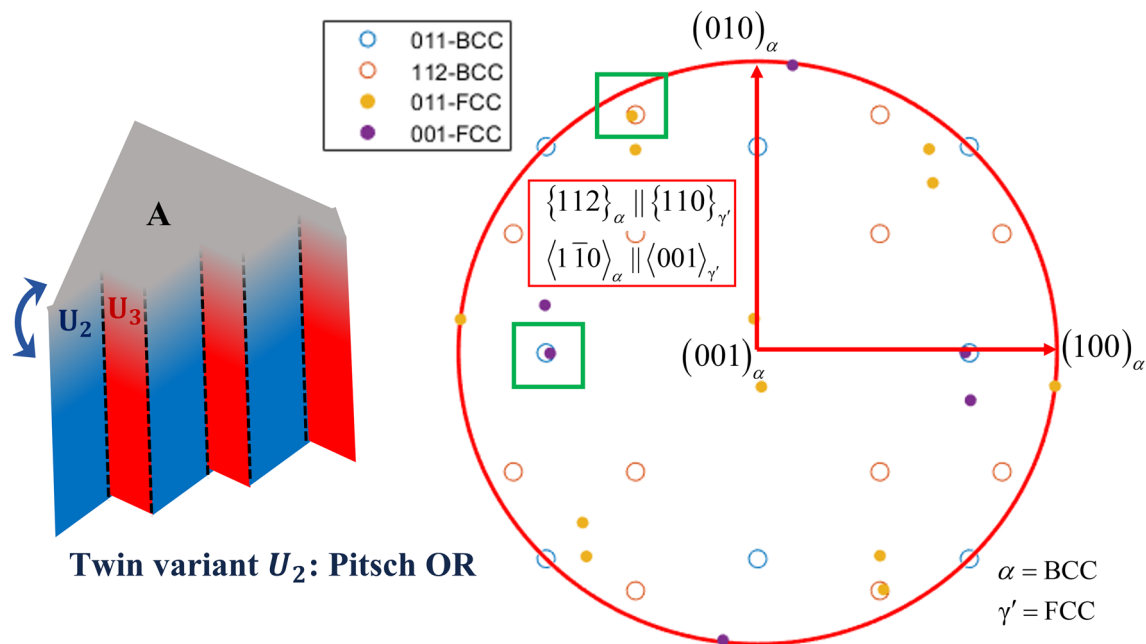


Fig. 7 Predictions of relative orientations between twin-variant (with stretch) U_2 and the parent austenite, explaining the Pitsch OR

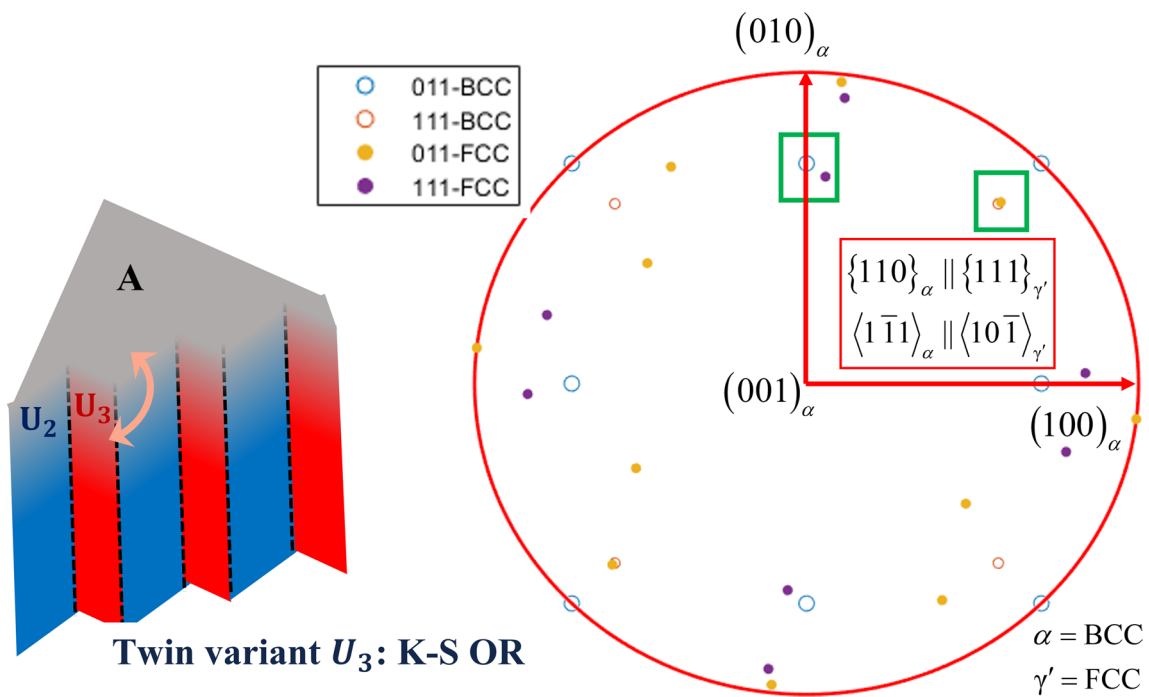


Fig. 8 Predictions of relative orientations between the second twin-variant (with stretch) U_3 and the parent austenite, explaining the Kurdjumov–Sachs OR

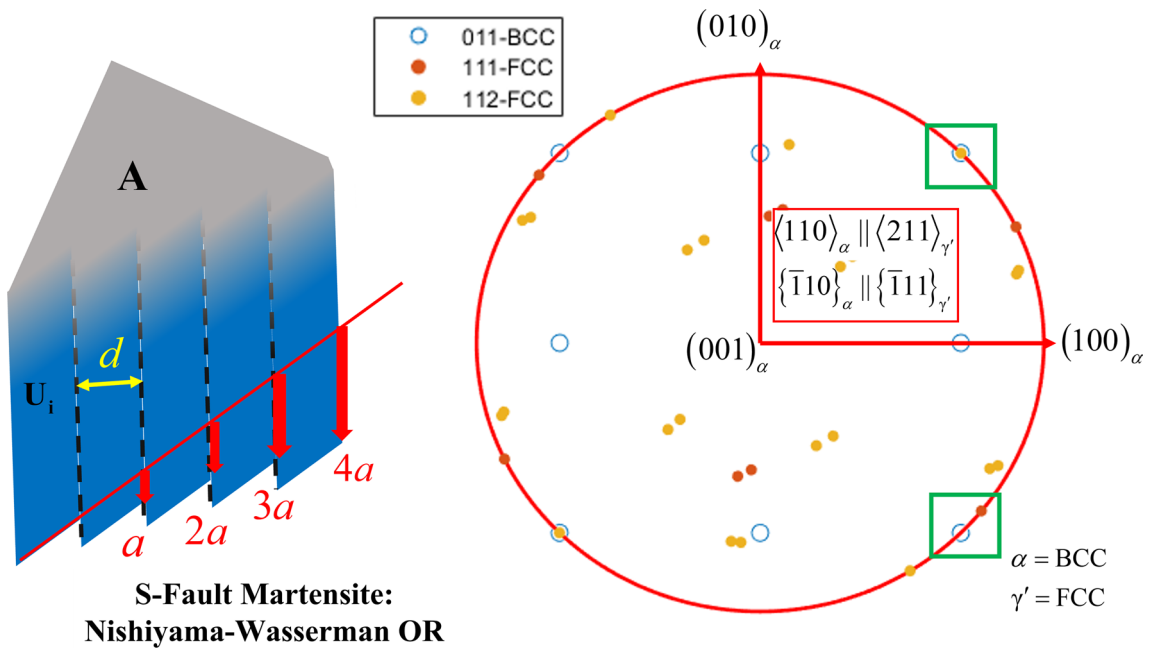


Fig. 9 Predictions of relative orientations between the stacking-faulted martensitic variant (with stretch) U_i and the parent austenite, explaining the Nishiyama–Wassermann OR

$$\mathbf{F}_{Mi} = \mathbf{R}_h \left[\mathbf{U}_i + \left(\frac{1}{d} \right) (\vec{a} \otimes \hat{n}) \right] = \mathbf{I} + \vec{b} \otimes \hat{m} \quad (16)$$

where \mathbf{R}_h is a rotation tensor, \mathbf{I} is the identity tensor, \vec{b} is the effective transformation shear of the IPS deformation and \hat{m} is the habit plane of the transformation.

For a given variant \mathbf{U}_i , the slip-plane is given by $\hat{n}_{FCC} \in 1/\sqrt{3}\{111\}$ and $\vec{a}_{FCC} \in s/\sqrt{6}\langle 112 \rangle$, where $s = 1/\sqrt{2}$, comprising a total of 12 slip systems. The normal vector \hat{n} and fault-shear \vec{a} are given by:

$$\hat{n} = \frac{\mathbf{U}_i (\mathbf{Q}_i^{ROT})^T \hat{n}_{FCC}}{\|\mathbf{U}_i (\mathbf{Q}_i^{ROT})^T \hat{n}_{FCC}\|}; \vec{a} = \frac{(\mathbf{Q}_i^{ROT})^T \vec{a}_{FCC}}{\|\mathbf{U}_i^{-1} \hat{n}_{FCC}\|} \quad (17)$$

Note that Eq. (16) is identical to (10) if we redefine $d = 1/f$. Therefore, Eq. (16) can be solved following the same method as solving (10), for a given variant \mathbf{U}_i , and for a given Shockley-partial slip system defined by \vec{a} and \hat{n} . It is found that 24 independent HPV solutions exist, which are also the same family of habit planes $\{0.1678, 0.6455, 0.7451\}$. Therefore, the same HPVs can form with either an internally twinned morphology (with 2 twin variants \mathbf{U}_i and \mathbf{U}_j) or stacking-faulted morphology (with a single variant \mathbf{U}_i). Considering one of the HPV solutions in this family of stacking-faulted solutions, say with $i = 1$, the deformation gradient \mathbf{F}_{M1} is calculated from (16). Following the same procedures for computing the error-functions and plotting the stereographic projections as described in Sect. “[Theoretical Predictions: Twinned Martensite](#),” it is found that the stacking-faulted variant obeys the Nishiyama-Wassermann OR (shown in Fig. 9b). Thus, all observations of ORs have been explained from a theoretical standpoint.

Discussion

A fundamental knowledge-gap in understanding of martensitic transformations lies in the interpretation of the Orientation Relationship (OR) between the parent Austenite (A) and product Martensite (M) phase. Thorough knowledge of these ORs are a prerequisite to construct and understand behavior of the A-M transformation front. Such an understanding will ultimately help uncover the unknown mechanisms of slip-emission at these interfaces. These relationships have been proposed for several SMAs and it can often be a tacit presumption that these relationships are “exact” and are unique for a specific SMA system. In this study, experimental results on FeMnNiAl show that multiple ORs are possible, independently observing a combination of the Nishiyama-Wassermann OR, the Pitsch OR, and the Kurdjumov–Sachs OR. And in all the results, it is obvious that the ORs are not obeyed exactly but only within a certain

tolerance of mismatch, of the order of few degrees. This can be observed in the lacking coincidence of the TEM diffraction spots in Fig. 2c or of the points on the stereographic projections in Fig. 5. Although it must be mentioned that the alignment is still close, evidenced by the high proximity of the spots/points. Given these results, the focus is to address the origin of these multiple ORs based on the morphology of the underlying martensitic structure.

The modeling approach applies the energy-minimization theory of martensite to predict the ORs. This is a continuum theory that is generally used to predict the irrational Miller indices of the habit planes of the transformation. In this study, the same theory is combined with the crystallography of the transformation, involving the Bain lattice correspondences to predict the OR. The OR is clearly shown to depend on the internal morphology of martensite whether twinned or stacking-faulted. If the martensite is twinned, then the individual twin variants explain the Pitsch and Kurdjumov–Sachs ORs. And if the martensite is stacking-faulted, the Nishiyama-Wassermann OR is explained. Additionally, it is proposed that the effective rotation \mathbf{R}_h in both morphologies has a role to play [Eqs. (10) and (16)], and this rotation comes about to ensure the martensite follows an Invariant Plane-Strain (IPS) deformation. Therefore, there is an additional misorientation introduced in the variants in an effort by the martensite to minimize its strain-energy via formation on an invariant irrational plane (i.e., the habit plane). Further, the prediction of the theory checks the OR by computing finite-valued error-functions as discussed in 2.2. In that sense, the question is not which exact OR is followed but rather which OR is followed to the “nearest extent” (therefore least error Δe) by the martensite. And by this interpretation it is plausible to expect the material to exhibit more than one OR as it only describes the nearest rotational orientation relation between the planes and directions of both A and M phases.

This study also develops a novel theory for stacking-faulted martensite, for the first time in literature to the best of the authors’ knowledge. The stacking-faulted structure appends an additional shear $1/d(\vec{a} \otimes \hat{n})$ to the single variant \mathbf{U}_i . Once this understanding is reached it becomes clear that the HPV solution for this morphology can be obtained analogously to the twinned case, as mentioned in Sect. “[Theoretical Predictions: Stacking-Faulted Martensite](#).” The predictions are consistent with the experimental results where existence of stacking-faults in the martensite is evidenced in Fig. 2e. It is interesting to note that given the one–one correspondence between the OR and the underlying substructure of the martensite, the observed OR can be used as a marker to identify the underlying martensitic morphology as either twinned or stacking-faulted.

Conclusion

There are two key knowledge-gaps in the understanding and interpretation of these ORs. The first is regarding the exactness of these relationships. The second is regarding its uniqueness for a given material, where in fact it depends on the internal morphology of martensite. In this study, experimental research for the first time showed 3 distinct ORs for transforming FeMnNiAl (BCC to FCC transformation) Shape Memory Alloy. They are the Kurdjumov–Sachs, Nishiyama–Wassermann and Pitsch ORs. Observations of such a non-unique OR poses a basic question of whether the OR is a material property or if it can evolve depending on other microstructural factors. A theoretical treatment to predict these ORs is undertaken. It is shown that the OR depends on the internal microstructural morphology of the martensitic phase. Depending on whether the morphology corresponds to a twinned structure or stacking-faulted structure, the OR can vary. When the martensite is internally twinned, it exhibits two twin variants with a distinct twin plane. One of the variants reproduces the Pitsch OR and the other variant results in the Kurdjumov–Sachs OR. When the martensite involves stacking-faults, the corresponding single variant sustaining the faults is shown to reproduce the Nishiyama–Wassermann OR. A novel theoretical framework underlying the predictions for stacking-faulted martensite was developed for this purpose. It is shown that these ORs are not exact and there exists a non-trivial tolerance in the parallelism relations that have been proposed thus far, of the order of few degrees. It is crucial to know of the existence of such a tolerance as it dictates how the A and M lattices are oriented relative to each other and how the transformation front between them can behave during the transformation.

Acknowledgements The work was initially supported by the Air Force Office of Scientific Research (AFOSR) under award number FA9550–18–1–0198 and later by the National Science Foundation (NSF-DMR) under award number 2104971, which is gratefully acknowledged.

Data Availability Not applicable.

References

- Wei S, He F, Tasan CC (2018) Metastability in high-entropy alloys: a review. *J Mater Res* 33(19):2924–2937
- Zhang JL, Tasan CC, Lai MJ, Yan D, Raabe D (2017) Partial recrystallization of gum metal to achieve enhanced strength and ductility. *Acta Mater* 135:400–410
- Stemper L, Tunes MA, Dumitraschkewitz P, Mendez-Martin F, Tosone R, Marchand D, Curtin WA, Uggowitzer PJ, Pogatscher S (2021) Giant hardening response in AlMgZn(Cu) alloys. *Acta Mater* 206:116617
- Akamine H, Mitsuhara M, Nishida M, Samaev V, Schryvers D, Tsukamoto G, Kunieda T, Fujii H (2021) Precipitation behaviors in Ti–2.3 Wt Pct Cu alloy during isothermal and two-step aging. *Metall Mater Trans A* 52(7):2760–2772
- Abueidda DW, Almasri M, Ammourah R, Ravaoli U, Jasiuk IM, Sobh NA (2019) Prediction and optimization of mechanical properties of composites using convolutional neural networks. *Compos Struct* 227:111264
- Chawla KK (2012) Micromechanics of composites. In: Chawla KK (ed) *Composite materials: science and engineering*. Springer, New York, pp 337–385
- Zhang K, Surana M, Haasch R, Tawfick S (2020) Elastic modulus scaling in graphene-metal composite nanoribbons. *J Phys D Appl Phys* 53(18):185305
- Sidharth R, Mohammed ASK, Abuzaid W, Sehitoglu H (2021) Unraveling frequency effects in shape memory alloys: NiTi and FeMnAlNi. *Shape Memory Superelasticity* 7(2):235–249
- Abuzaid W, Sehitoglu H (2019) Shape memory effect in FeMn–NiAl iron-based shape memory alloy. *Scripta Mater* 169:57–60
- Bucsek AN, Hudish GA, Bigelow GS, Noebe RD, Stebner AP (2016) Composition compatibility, and the functional performances of ternary NiTiX high-temperature shape memory alloys. *Shape Memory Superelasticity* 2(1):62–79
- Maeshima T, Ushimaru S, Yamauchi K, Nishida M (2006) Effect of heat treatment on shape memory effect and superelasticity in Ti–Mo–Sn alloys. *Mater Sci Eng, A* 438–440:844–847
- Duerig T, Pelton A, Stöckel D (1999) An overview of nitinol medical applications. *Mater Sci Eng, A* 273–275:149–160
- Mohd Jani J, Leary M, Subic A, Gibson MA (2014) A review of shape memory alloy research, applications and opportunities. *Mater Des* 56:1078–1113
- Kumar PK, Lagoudas DC (2008) Introduction to shape memory alloys, shape memory alloys: modeling and engineering applications. Springer, Boston, pp 1–51
- Otsuka K, Sawamura T, Shimizu K (1971) Crystal structure and internal defects of equiatomic TiNi martensite. *Physica Status Solidi* 5(2):457–470
- Knowles KM, Smith DA (1981) The crystallography of the martensitic transformation in equiatomic nickel-titanium. *Acta Metall* 29(1):101–110
- Madangopal K (1997) The self accommodating martensitic microstructure of NiTi shape memory alloys. *Acta Mater* 45(12):5347–5365
- Güler E, Kirindi T, Aktas H (2007) Comparison of thermally induced and deformation induced martensite in Fe–29% Ni–2% Mn alloy. *J Alloy Compd* 440(1):168–172
- Sari U, Güler E, Kirindi T, Dikici M (2009) Characterization of martensite in Fe–25%Ni–15%Co–5%Mo alloy. *J Phys Chem Solids* 70(8):1226–1229
- Sari U, Kirindi T (2008) Effects of deformation on microstructure and mechanical properties of a Cu–Al–Ni shape memory alloy. *Mater Charact* 59(7):920–929
- Matsuda M, Kiwaki K, Akamine H, Nishida M (2022) Effect of Hf on the microstructure and martensitic transformation behavior in Ti–Pd–Hf alloy. *J Alloy Compd* 917:165491
- Inamura T, Nishiura T, Kawano H, Hosoda H, Nishida M (2012) Self-accommodation of B19' martensite in Ti–Ni shape memory alloys Part III Analysis of habit plane variant clusters by the geometrically nonlinear theory. *Philos Mag* 92(17):2247–2263
- Mohammed ASK, Sehitoglu H (2020) Martensitic twin boundary migration as a source of irreversible slip in shape memory alloys. *Acta Mater* 186:50–67
- Kajiwara S (1999) Characteristic features of shape memory effect and related transformation behavior in Fe-based alloys. *Mater Sci Eng A* 273–275:67–88
- Hamilton RF, Sehitoglu H, Chumlyakov Y, Maier HJ (2004) Stress dependence of the hysteresis in single crystal NiTi alloys. *Acta Mater* 52(11):3383–3402

26. Norfleet DM, Sarosi PM, Manchiraju S, Wagner MFX, Uchic MD, Anderson PM, Mills MJ (2009) Transformation-induced plasticity during pseudoelastic deformation in Ni–Ti microcrystals. *Acta Mater* 57(12):3549–3561
27. Simon T, Kröger A, Somsen C, Dlouhy A, Eggeler G (2010) On the multiplication of dislocations during martensitic transformations in NiTi shape memory alloys. *Acta Mater* 58(5):1850–1860
28. Zhang J, Somsen C, Simon T, Ding X, Hou S, Ren S, Ren X, Eggeler G, Otsuka K, Sun J (2012) Leaf-like dislocation substructures and the decrease of martensitic start temperatures: a new explanation for functional fatigue during thermally induced martensitic transformations in coarse-grained Ni-rich Ti–Ni shape memory alloys. *Acta Mater* 60(5):1999–2006
29. Sidharth R, Wu Y, Brenne F, Abuzaid W, Sehitoglu H (2020) Relationship between functional fatigue and structural fatigue of iron-based shape memory alloy FeMnNiAl. *Shape Memory Superelasticity* 6(2):256–272
30. Omori T, Ando K, Okano M, Xu X, Tanaka Y, Ohnuma I, Kainuma R, Ishida K (2011) Superelastic effect in polycrystalline ferrous alloys. *Science* 333(6038):68–71
31. Xia J, Noguchi Y, Xu X, Odaira T, Kimura Y, Nagasako M, Omori T, Kainuma R (2020) Iron-based superelastic alloys with near-constant critical stress temperature dependence. *Science* 369(6505):855–858
32. Abuzaid W, Wu Y, Sidharth R, Brenne F, Alkan S, Vollmer M, Krooß P, Niendorf T, Sehitoglu H (2019) FeMnNiAl iron-based shape memory alloy: promises and challenges. *Shape Memory Superelasticity* 5(3):263–277
33. Ojha A, Sehitoglu H (2016) Transformation stress modeling in new FeMnAlNi shape memory alloy. *Int J Plast* 86:93–111
34. Vallejos JM, Sobrero CE, Ávalos M, Signorelli JW, Malarría JA (2018) Crystallographic orientation relationships in the $\alpha \rightarrow \gamma'$ martensitic transformation in an Fe–Mn–Al–Ni system. *J Appl Crystallogr* 51(4):990–997
35. Leineweber A, Walnsch A, Fischer P, Schumann H (2021) Crystallography of Fe–Mn–Al–Ni shape memory alloys. *Shape Memory Superelasticity* 7(3):383–393
36. Kelly PM (2012) 1 - Crystallography of martensite transformations in steels. In: Pereloma E, Edmonds DV (eds) *Phase transformations in steels*. Woodhead Publishing, Sawston, pp 3–33
37. Ball JM, James RD (1987) Fine phase mixtures as minimizers of energy. *Arch Ration Mech Anal* 100(1):13–52
38. Zhang X, Sehitoglu H (2004) Crystallography of the $B2 \rightarrow R \rightarrow B19'$ phase transformations in NiTi. *Mater Sci Eng, A* 374(1):292–302

Publisher's Note Springer Nature remains neutral with regard to jurisdictional claims in published maps and institutional affiliations.

Springer Nature or its licensor (e.g. a society or other partner) holds exclusive rights to this article under a publishing agreement with the author(s) or other rightsholder(s); author self-archiving of the accepted manuscript version of this article is solely governed by the terms of such publishing agreement and applicable law.